Biogeosciences
Discussions

Air–sea carbon flux from high-temporal-resolution data of in situ CO_2 measurements in the southern North Sea

Steven Pint[1], Gert Everaert[1], Hannelore Theetaert[1], Michiel B. Vandegehuchte[1], Thanos Gkritzalis[1]

[1] Flanders Marine Institute, Wandelaarkaai 7, B-8400, Ostend, Belgium

5   *Correspondence to*: Steven Pint (steven.pint@vliz.be), Thanos Gkritzalis (thanos.gkritzalis@vliz.be)

Abstract. An important element to keep track of global change is the atmosphere–water exchange of carbon dioxide (CO_2) in the ocean as it provides insight in how much CO_2 is incorporated in the ocean (i.e. the ocean as a sink for CO_2) or emitted to the atmosphere (i.e. the ocean as a source). To date, only few high-resolution observation sets are available to quantify the spatiotemporal variability of air–sea CO_2 fluxes. In this study, we used observations of pCO_2 collected daily at the ICOS station

10   Thornton Buoy in the southern North Sea from February until December 2018 to calculate air–sea CO_2 fluxes. Our results show a seasonal variability of the air–sea carbon flux, with the sea being a carbon sink from February until June switching to a carbon source in July and August, before switching back to a sink until December. We calculated that the sink was largest in April (-0.95 ± 0.90 mmol C m^{-2} d^{-1}), while in August, the source was at its maximum (0.08 ± 0.13 mmol C m^{-2} d^{-1}). On an annual basis, we found a sink for atmospheric CO_2 of 130.19 ± 149.93 mmol C m^{-2} y^{-1}. Apart from region- and basin-scale

15   estimates of the air–sea CO_2 flux, also local measurements are important to grasp local dynamics of the flux and its interactions with biogeochemical processes.

1 Introduction

Increased anthropogenic emissions of greenhouse gases (GHGs) lead to global warming (IPCC, 2019), and observing their balance is an important way to keep track of global change (Steinhoff et al., 2019). A key element in this balance is the air–

20   sea exchange of CO_2 in the ocean, as the oceans are responsible for the uptake of 25% of anthropogenic CO_2 emissions (Friedlingstein et al., 2019). The air–sea CO_2 flux provides insight in how much CO_2 is added to the marine environment from the atmosphere (i.e. the sea being a sink for atmospheric CO_2) or emitted by the marine environment to the atmosphere (i.e. the sea being a source). The North Atlantic Ocean is one of the major sinks with an uptake of 680 mmol C m^{-2} y^{-1} (Watson et al., 2009) in 2005, and between 800 and 4000 mmol C m^{-2} y^{-1} (Woolf et al., 2019) in 2010. Continental shelfs are regarded as

25   sinks of carbon with an average air–sea CO_2 rate of 1900 mmol C m^{-2} y^{-1} for the European continent (Borges et al., 2006). However, the Southern Bight of the North Sea (SBNS), i.e. a European shelf sea, is shown as a source area in Thomas et al. (2004). The latter is in contrast with other studies that suggest that the SBNS and the whole North Sea can be regarded as a sink for CO_2 (Borges and Frankignoulle, 2002; Laruelle et al., 2018; Schiettecatte et al., 2007). The southern part of the North Sea includes the Belgian Continental Shelf (BCS), which is a well-studied area in terms of air–sea surface dynamics and carbon

30   biogeochemical cycling (e.g. Borges et al., 2019; Gypens et al., 2011, 2004). In terms of air–sea carbon fluxes, the BCS shifted from being a carbon source in the 1950s to a carbon sink in the 1980s (Gypens et al., 2009), with more recent source-sink turnovers (Gypens et al. 2011). Changing seawater physical and biogeochemical characteristics in the BCS result in seasonal patterns of air-sea CO_2 flux (Gypens et al., 2004, 2011). The dynamic nature of the BCS in terms of annual CO_2 fluxes, which were often based on short term measurements and simulated values in past studies, highlight the necessity of high-resolution

35   robust CO_2 observations. Therefore, in the present study, we monitored the local dynamics of CO_2 flux using high-temporal-resolution data of both partial pressure of CO_2 in the sea ($pCO_{2, sea}$) and in the air ($pCO_{2, air}$). Our aims were to quantify the air–sea carbon flux, to identify what drives the seasonality of the flux in a specific year and to identify the annual source–sink dynamics in a specific location of the BCS.

2 Materials and methods

40   The North Sea has a surface of 670.000 km² (EEA, 2015) of which the Belgian Continental Shelf (BCS) occupies about 0.5% (or 3.454 km²; Belpaeme et al., 2011). The BCS is relatively shallow with water depths gradually increasing to 45m from the Southeast towards the Northwest (Van Lancker et al., 2015). Apart from extreme observations, surface water temperatures vary seasonally between 5°C and 20°C. The salinity is strongly influenced by the river plumes of the Scheldt, Rhine, Seine and Meuse (Lacroix et al., 2004) and varies between 29 to 35 PSU.
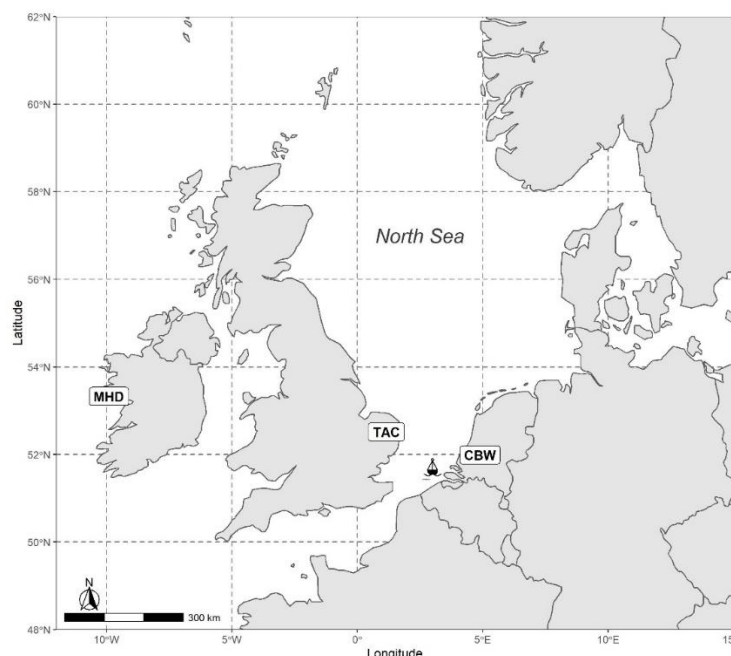
45

Figure 1: Map of the North Sea with the location of the Thornton Buoy indicated by the buoy symbol. The locations of the ICOS atmospheric stations, i.e. Cabauw (CBW), Tacolneston (TAC) and the atmospheric station, i.e. Mace Head (MHD) are also presented.

50   The Flanders Marine Institute is operating the Fixed Ocean Station "BE-FOS-VLIZ Thornton Buoy" in this area as part of the European research infrastructure "Integrated Carbon Observation System" (ICOS - ERIC, https://www.icos-cp.eu/). The station is equipped with commercial sensors to measure in-situ the sea surface xCO_2, atmospheric xCO_2, sea surface Temperature (SST), sea surface salinity (SSS) and the total gas pressure of CO_2. The BE-FOS-VLIZ Thornton Buoy is located approximately 30 km away from Zeebrugge in the area of the Thornton bank wind turbine farm (51.579N, 2.993E; Fig. 1). In

55   this study, we used observations from the year 2018. A schematic of the mooring and position of the sensors is depicted in Figure A1. The equipment details and data collection information are listed in Table 1.

Table 1: Details of the in situ sensors on the BE-FOS-VLIZ Thornton Buoy and wind data collected from Meetnet Vlaamse Banken. The sensor (if available), sensor supplier, accuracy and sampling frequency are given for the following parameters; sea surface
60   **salinity (SSS), sea surface temperature (SST), wind speed and partial pressure of both oceanic ($pCO_{2, sea}$) and atmospheric CO_2 ($pCO_{2, air}$).**

Parameter	Sensor	Sensor supplier	Accuracy	Sampling frequency
SSS	SBE37-SMP-ODO	Seabird Scientific	$\pm$ 0.01 PSU	15 min
SST	SBE37-SMP-ODO	Seabird Scientific	$\pm$ 0.001 ℃	15 min
Wind speed	-		$\pm$ 0.1 m s^{-1}	10 min
$pCO_{2, sea}$	CO2-PRO ATM	Pro-Oceanus Systems Inc	$\pm$ 10 µatm	4 h
$pCO_{2, air}$	CO2-PRO ATM	Pro-Oceanus Systems Inc	$\pm$ 1 µatm	4 h

All the sensors (Table 1) are connected to a data logger (CR6, Campbell Scientific) which has a dedicated WiFi connection with a nearby wind turbine (approx. 250 m away). The wind turbine is connected to the managing company's servers (C-Power) via underground optic fibre cables and there is secure Ethernet connection with the VLIZ servers. This allows secure

65   and robust 2-way interactive communication with the buoy system and individual sensors, and provides the means to adapt sampling strategies of the sensors and identify issues very effectively.

The sensors used for this study (SBE37-SMP-ODO and CO2-PRO ATM) are calibrated by the manufacturers once per year. Additionally the pCO_2 measurements of the buoy were validated monthly against calculated pCO_2 values from measurements of Total Dissolved Inorganic Carbon (CT), Total Alkalinity (TA) and pH of manually collected samples. Water sampling

70   followed the SOP1 described in Dickson et al. (2007). TA, CT and pH were determined using the methodologies described in Dickson et al. (2007). For TA the method follows SOP3b of Dickson et al. (2007; commercially available system VINDTA 3s). The pH analysis and setup follows SOP6a (Dickson et al., 2007) using the Thermo Scientific Orion pH meter (STAR A211) and ROSS Sure Flow glass body pH electrode and we report pH at Total Scale at 25℃ as measurements are performed in a thermostatic environment (Grant Water Bath). Total Dissolved Inorganic Carbon (CT) is determined using the

75   commercially available Automated Infra Red Carbon Analyzer (AIRICA). For all methods, we use CRMs from Scripps Institute of Oceanography (UCSD). The uncertainties for each method are mentioned in Table 2. For the calculation of $pCO_{2, sea}$, we have used the R package 'seacarb' (Gattuso et al., 2020).

The calculated pCO$_{2, sea}$ values were used to calibrate the sensor data using a linear regression method (Fig. A2). The SST and

80   SSS data of the buoy were validated against data obtained from RV Simon Stevin's CTD system (SBE3 & SBE4, respectively for SST & SSS - Seabird Scientific) and underway Thermo-Salinograph sensor (SBE21 - Seabird Scientifics) when visiting the station and collecting samples. The pCO$_{2, air}$ measurements were evaluated against xCO$_2$ data from nearby ICOS atmospheric stations on land. For this comparison, we used the non-parametric Kruskal–Wallis rank sum test and the pairwise Wilcoxon Rank Sum test in the R package 'stats' (R Core Team, 2019).

85   **Table 2: Summary of analytical methods for analysis of spot samples**

Parameter	System	System supplier	Accuracy
Total Dissolved Inorganic Carbon (C$_T$)	AIRICA	Marianda	± 2.5 µmol kg^{-1}
Total Alkalinity (TA)	VINDTA 3s	Marianda	± 2.0 µmol kg^{-1}
pH (TS @ 25°C)	EMF method (Glass electrode + pH meter)	ThermoFisher	± 0.0025

The air–sea CO$_2$ flux (F) is calculated (Eq. 1) according to the wind-driven turbulence diffusivity model of Nightingale et al. (2000) expressed in partial pressure:

$$F = k_{Nightingale} \cdot K_0 \cdot (pCO_{2,sea} - pCO_{2,air}) \tag{1}$$

where k$_{Nightingale}$ is the gas transfer velocity (length · time^{-1}, Eq. 2), K$_0$ is the solubility of CO$_2$ in seawater (mass · volume^{-1} ·

90   pressure^{-1}) and pCO$_{2, sea}$ and pCO$_{2, air}$ are the partial pressure of CO$_2$. We calculated pCO$_2$ by multiplying xCO$_2$ measurements with the total gas pressure of CO$_2$ respectively in seawater or atmosphere. The solubility of CO$_2$ in seawater depends on the sea surface temperature (SST) and the sea surface salinity (SSS; Wanninkhof, 2014). The gas transfer velocity of Nightingale et al. (2000) uses wind speed measured at 10 m height (U$_{10m}$).

$$k_{Nightingale} = 0.222 \cdot U_{10m}^2 + 0.333 \cdot U_{10m} \tag{2}$$

95   Wind speed (10m above sea level) data were acquired from Meetnet Vlaamse Banken (MVB) for the Westhinder platform, Wandelaar platform and Scheur Wielingen platform, which are located approximately 20 km to 40 km more to the South and Southwest. Wind speed was measured every ten minutes. In the SST and SSS records, there are no data in September 2018 due to a malfunction in the buoy's SBE37-SMP-ODO sensor. To account for the lacking SSS data, we completed our times series with salinity data from by the RV Simon Stevin's CTD system in the same period (Flanders Marine Institute, 2019).

100   The SST data gaps were completed by data from a second water temperature sensor installed on an Aanderaa Seaguard multiparametric platform (Fig. A1b). Timestamps were used in order to combine data sets from various sensors and systems. All data were assessed for potential outliers. As in Salgado et al. (2016), outliers were defined as values lying outside the borders of the lower quartile minus three times the interquartile range (Q$_{25}$ – 3*IQR) and the upper quartile plus three times the interquartile range (Q$_{75}$ + 3*IQR). The daily mean air–sea CO$_2$ flux was calculated from 1891 time points. We took the

105   day–night cycle of the CO$_2$ flux into account by using daily means. Besides, we calculated monthly means and standard

Biogeosciences
Discussions

deviation. Our data covers the period from February 2018 until December 2018. To quantify the annual CO_2 flux based on eleven months of data, we calculated a weighted mean for the winter, i.e. February and December, and the remaining nine months, respectively, using weights 0.25 and 0.75. We, then, extrapolated the weighted mean to a year. A summary of the input data is provided in Table 3. We investigated if the CO_2 flux calculated with $xCO_{2, air}$ from the Thornton Buoy was

110 different from the CO_2 fluxes based on $xCO_{2, air}$ measurements at nearby atmospheric stations (Sect 3.1). We compared them using the non-parametric Kruskal–Wallis rank sum test and the pairwise Wilcoxon Rank Sum test in the R package 'stats' (R Core Team, 2019).

Table 3: Summary statistics of the variables, i.e. sea surface salinity (SSS), sea surface temperature (SST), wind speed and partial
115 **pressure of both oceanic ($pCO_{2, sea}$) and atmospheric CO_2 ($pCO_{2, air}$) that were used to calculate air–sea CO_2 flux. In total, we used 1891 measurements of each variable in this study.**

Parameter	Min	Max	Mean
SSS (PSU)	32.1	34.7	33.4
SST (°C)	3.3	22.2	13.4
Wind speed (m s^{-1})	0.3	17.9	6.8
$pCO_{2, sea}$ (µatm)	126.9	525.6	337.8
$pCO_{2, air}$ (µatm)	389.4	464.7	418.0

We adopted the method developed by Takahashi et al. (2002) to separate and assess the seasonal effects of biological processes and temperature on pCO_2 and CO_2 flux dynamics over an annual cycle. We applied eq. 3 and 4, where T_{mean} is the mean annual temperature (13.4 °C) and T_{obs} is the in situ temperature. The relative importance of the components effects is expressed by

120 the thermal–biological ratio (T/B) or the difference (T-B), where T is $pCO_{2, therm}$ and B is $pCO_{2, bio}$.

$$pCO_{2, bio} = pCO_2 \cdot \exp(0.0423 \cdot (T_{mean} - T_{obs})) \tag{3}$$

$$pCO_{2, therm} = pCO_{2, mean\ annual} \cdot \exp(0.0423 \cdot (T_{obs} - T_{mean})) \tag{4}$$

A T/B ratio between zero and one implies the dominance of biological processes over thermal effects (T-B < 0), whereas a T/B ratio larger than one implies that temperature effects are dominant (T-B > 0).

125 **3 Results and discussion**

3.1 Environmental conditions

In 2018, sea surface salinity (SSS) varied between 32.1 PSU and 34.7 PSU (Fig. 2a) with a mean value of 33.4 ± 0.58 PSU. The water temperature followed a seasonal pattern with high temperatures in summer time (max. 22.2 °C) and low water temperatures during the winter (min. 3.3 °C; Fig. 2b). No seasonal pattern was observed for the wind speed, i.e. the wind speed

130 is highly variable throughout the year. The lowest wind speed measured was 0.3 m s^{-1} and the highest was 17.9 m s^{-1} (Fig. 2c).

The $pCO_{2, air}$ fluctuated between 389.4 µatm and 464.7 µatm (Fig. 2d). The $pCO_{2, sea}$ data were validated against calculated values of $pCO_{2, sea}$ from DIC and pH values of manually collected samples. After that the $pCO_{2, sea}$ data were corrected with a linear regression method and validated against the manually collected (spot) samples. The $pCO_{2, sea}$ had a large range (126.9 µatm – 525.6 µatm), and reached its lowest value in May and highest value in August (Fig. 2d).
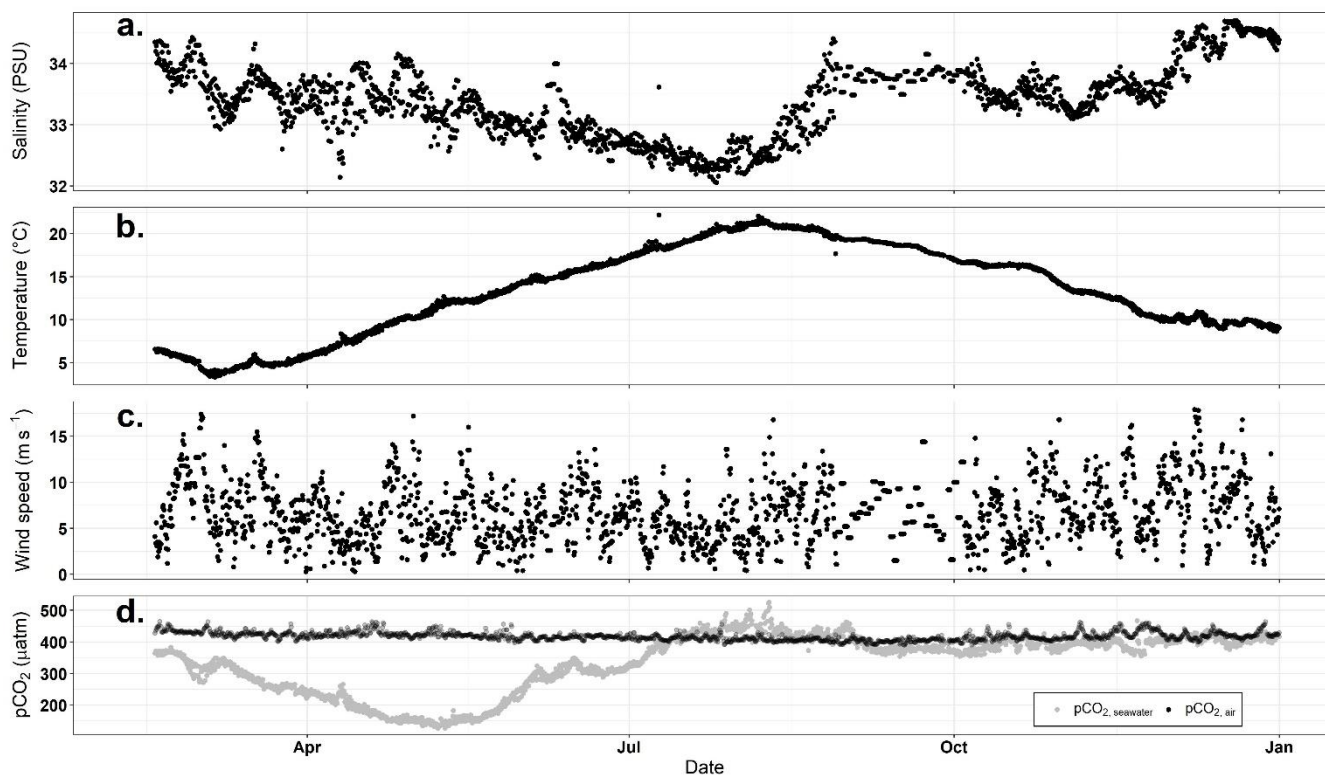

135

Figure 2: All observations used in this study to calculate CO2 fluxes: (a) salinity, (b) temperature, (c) wind speed and (d) pCO₂ of seawater (black) and air (grey). The 1891 observations for each variable are given in chronological order from February 2018 to December 2018. The x–axis is the same for the different variables. All observations went through a quality control and correction to address and eliminate possible outliers from this study.

140   These observed $pCO_{2, sea}$ concentrations corroborate with data found by Gypens et al. (2011) and Borges et al. (2006) for the English Channel (ECH) and the Southern Bight of the North Sea (SBNS). Borges et al. (2006) found that the spring bloom in early spring was followed by an increase in $pCO_{2, sea}$ in late spring–summer. Schiettecatte et al. (2007) observed that the SBNS was oversaturated in CO_2 during winter and strongly undersaturated in April–May. Schiettecatte et al. (2007) reported a minimum $pCO_{2, sea}$ value of 192.35 ± 35 µatm in the SBNS in April and a maximum of 455 ± 36 µatm in August. They

145   observed higher $pCO_{2, sea}$ values for the BCS, up to 900 µatm, but high values were measured close to the Scheldt plume (Schiettecatte et al., 2007). In the present research, we observed a seasonal trend of $pCO_{2, sea}$, which increased in the summer–early autumn and decreased in the winter–spring. We did not observe a strong seasonality in the $pCO_{2, air}$ record.

To evaluate our atmospheric xCO_2 data, we compared data from the BE-FOS-VLIZ Thornton Buoy with 2018 data from nearby (i.e. < 900 km) atmospheric stations (Fig. 3): i.e. two ICOS atmospheric stations Cabauw (207m above sea level;

150 Frumau et al., 2020) and Tacolneston (185m; O'Doherty et al., 2020) and one atmospheric station in Mace Head (24m; Delmotte et al., 2020). Usually, the CO_2 mole fraction data and products of these land-based atmospheric stations are used to calculate air–sea CO_2 fluxes, (e.g. Borges and Gypens, 2010). A basic comparison between the different data sets highlights the following. The minimum and maximum CO_2 mole fraction registered at the Thornton Buoy in 2018 was 389.4 ppm CO2 and 464.7 ppm CO_2. The atmospheric CO_2 mole fraction from sampling station Cabauw fluctuated between 394.0 ppm – 473.5

155 ppm CO_2, Tacolneston between 386.5 ppm – 455.1 ppm CO_2 and Mace Head between 394.2 ppm – 451.7 ppm CO_2. A similar trend was observed in the $xCO_{2, air}$ data of the Thornton Buoy as in the $xCO_{2, air}$ data of the other stations (Fig. 3). Our $xCO_{2, air}$ data is in range with the $xCO_{2, air}$ data of the land-based atmospheric stations (Fig. 3), which supports our use of local field observations. The use of local field observations of $xCO_{2, air}$ at sea provides useful information that complements the use of land-based stations because: 1) the sampling happens close to the water surface where the air–sea carbon exchange occurs,

160 and 2) the $xCO_{2, air}$ observations are more specific to the sampling location than land-based stations.
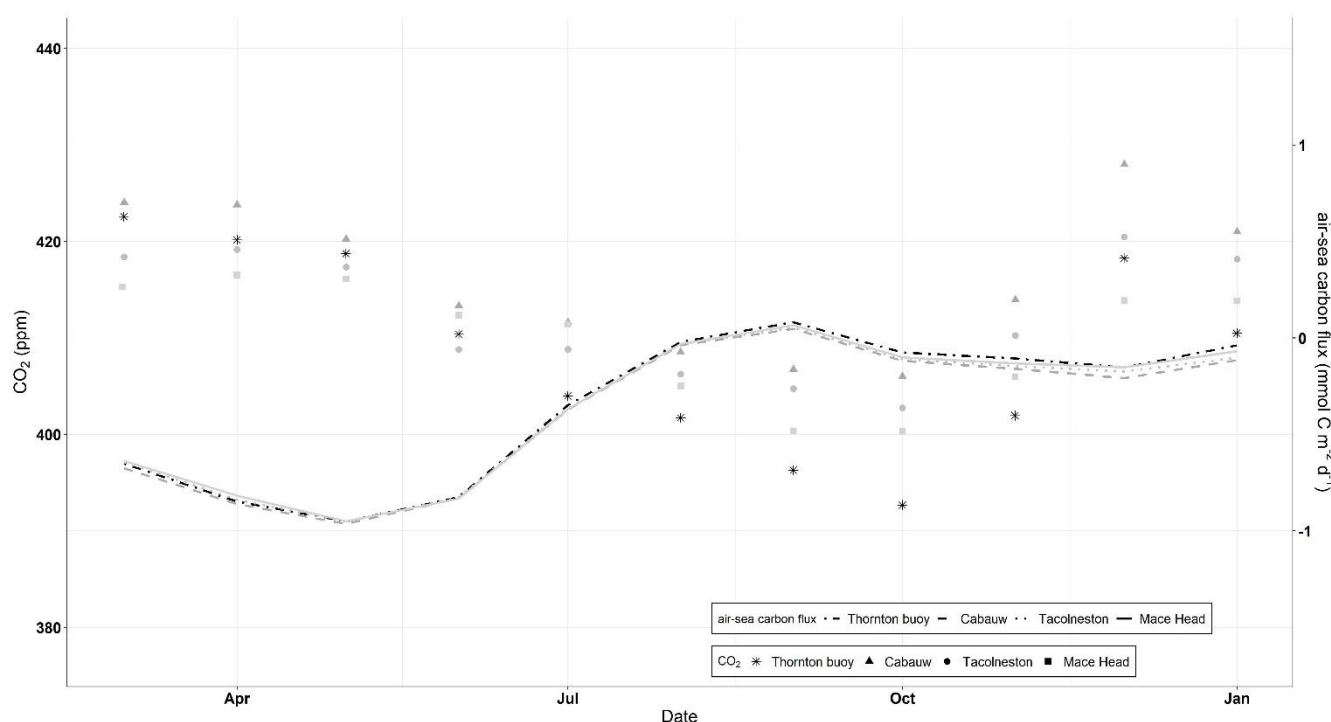
Figure 3: Monthly mean of the $CO_{2, air}$ data and air–sea CO_2 flux based on $pCO_{2, air}$ data from the atmospheric measuring stations (greyshades); Cabauw, Tacolneston, Mace Head, and the Thornton Buoy (black) are given in a chronological order, i.e. from February 2018 to December 2018, for our study period. Error bars were not included to make the figure clearer. The left axis is used
165 **for the CO_2 data and the right axis is used for the air–sea CO_2 flux.**

3.2 Air–sea CO2 flux

The air–sea CO_2 flux was estimated based on the salinity (Fig. 2a), temperature (Fig. 2b), wind speed (Fig. 2c), and pCO2 for seawater and atmosphere (Fig. 2d) time series at the Thornton Buoy in the BCS. We found that the wind speed had a large

impact on the magnitude of the CO_2 flux, i.e. higher wind speed increased the air–sea exchange of CO_2 in either way. The

170   daily means of the CO_2 flux varied between -2.99 mmol m^{-2} d^{-1} and 0.37 mmol m^{-2} d^{-1} (Fig. 4). We calculated monthly means

(-0.95 ± 0.90 mmol m^{-2} d^{-1} to 0.08 ± 0.13 mmol m^{-2} d^{-1}) and distinguished a clear seasonal pattern (Fig. 4). We compared these

air–sea CO_2 fluxes with air–sea CO_2 fluxes calculated with $pCO_{2, air}$ of the atmospheric stations. Only the carbon flux using the

atmospheric CO_2 data of Cabauw differed from the carbon flux using $pCO_{2, air}$ of the Thornton Buoy (p = 0.031; Fig.3), showing

the importance of local atmospheric pCO_2 measurements. Overall, the air–sea CO_2 flux calculated with different $pCO_{2, air}$

175   sources, i.e. Thornton Buoy and atmospheric stations, followed a very similar seasonal trend (Fig. 3).

Coinciding with other studies in the SBNS, we noted a seasonal effect in the air–sea carbon flux (Borges et al., 2006; Borges

and Gypens, 2010; Gypens et al., 2011; Kitidis et al., 2019; Schiettecatte et al., 2007). The BCS at our location acted as a

carbon sink from February until June (-0.95 ± 0.90 to -0.34 ± 0.23 mmol C m^{-2} d^{-1}; Fig. 4). The sink was the largest in April

with a monthly mean of 0.95 ± 0.90 mmol C m^{-2} d^{-1}. The flux direction switches to a weak carbon source from mid-July and
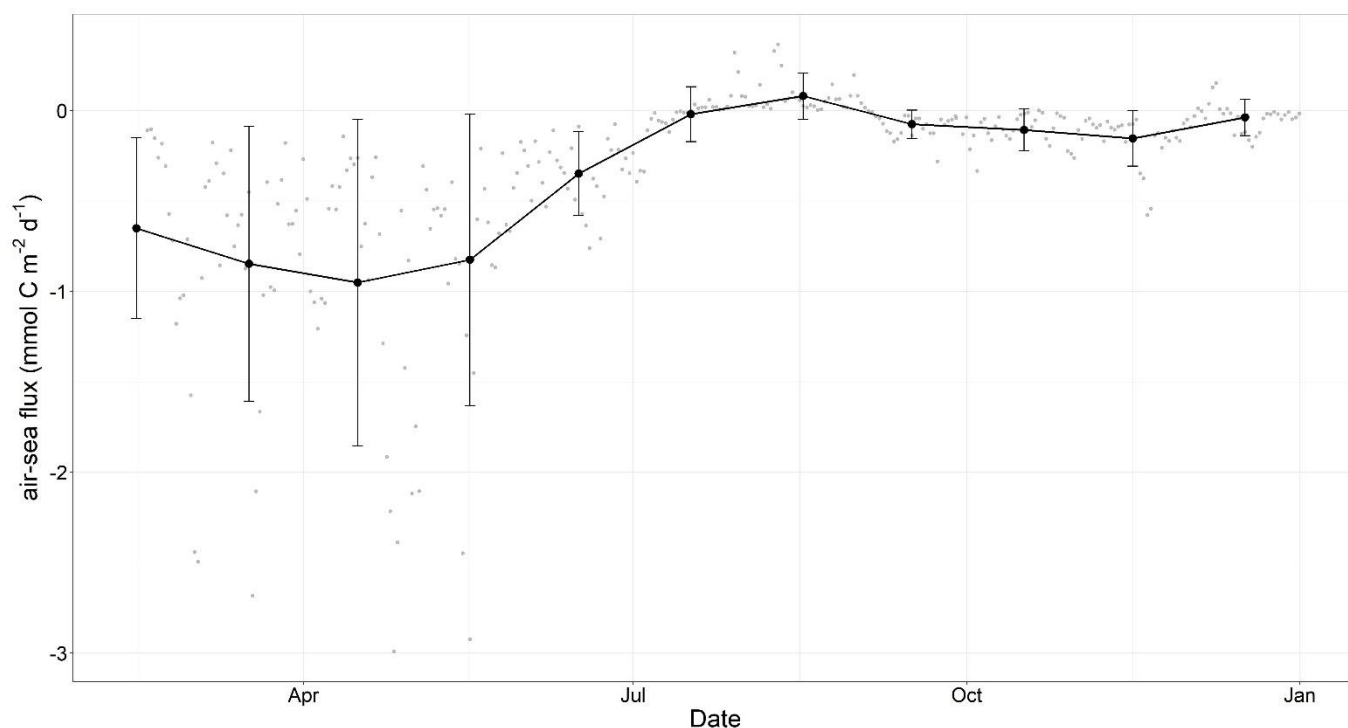

180

Figure 4: The daily means of air–sea CO_2 flux measurements (grey) and monthly means (black) with for the study period of February to December 2018 is shown in chronological order. Error bars represent the standard deviation on the monthly mean. The x-axis marks indicate the start of the month. Note that the monthly mean is given at the middle of the month.

until August with a monthly mean of 0.08 ± 0.13 mmol C m^{-2} d^{-1}. However, our findings contradict with the other studies from

185   August onwards. We found that the BCS at our measuring station switched back again to a small sink from September until

December (-0.15 ± 0.15 to -0.04 ± 0.10 mmol C m^{-2} d^{-1}; Fig. 4). We believe that the frequency and quality of our local

observations allowed us to identify the weak source in July and August, whereas it may have been unnoticed with different

observational capacity, e.g. sporadic sampling cruises. The Thornton Buoy ICOS setup allows for the collection of robust and high-frequency time series observations, , whereas sampling cruises can provide excellent spatial coverage however time

190 resolution can be sporadic (Borges and Frankignoulle, 2002; Schiettecatte et al., 2007). In that respect, it is possible that if samples and observations were obtained during a cruise in autumn over a relatively short period (days or weeks) when CO_2 was emitted, then the extrapolation of those observations could have led to the BCS being described as a source in autumn instead of a sink. We also need to acknowledge that environmental factors, e.g. temperature and biological activity can have significant effect on carbon fluxes (Gypens et al., 2011; Thomas et al., 2005, 2007; Wimart–Rousseau et al., 2020). Extreme

195 events, such as the heat wave in the summer of 2018, may have also contributed to some of the differences (e.g. increase in CO_2 concentrations) that we present in this study (Borges et al., 2019). Additionally, the solubility of CO_2 is lower in warmer water (Wiebe and Gaddy, 1940), reducing the uptake of atmospheric CO_2 (Yamamoto et al., 2018). Gypens et al. (2011) also simulated that the North Sea would change to a source for atmospheric CO_2 with warmer conditions (biological processes excluded). Other factors, such as wind and input of river plumes, are known to affect the air–sea carbon flux (Arndt et al.,

200 2011; Gypens et al., 2011; Laruelle et al., 2018; Nightingale et al., 2000; Thomas et al., 2005). High wind speed during the winter can amplify the CO_2-uptake in this season and so influence the yearly carbon exchange between the atmosphere and the sea (Kitidis et al., 2019). It is known that either temperature driven or biological processes are the dominant driving factor of the $pCO_{2, sea}$ (Schiettecatte et al., 2007; Thomas et al., 2005). In order to determine the main driver of the $pCO_{2, sea}$ dynamics, and as such to quantify the influence of temperature driven and biological processes on the observed CO_2 flux, we applied the

205 computational method of Takahashi et al. (2002).

We found that on an annual scale the biological activities dominated the $pCO_{2, sea}$ (T/B ratio = 0.69 and T-B = -113.32) and so CO_2 flux in the BCS. We also observed that the dominant factor changed by season. For the winter, i.e. February to March and October to December, we found that the thermal effect is dominant (T/B ratio = 1.24 and T-B = 42.28). However, in spring

210 and summer biological processes are dominant over the thermal effect (T/B ratio = 0.84 and T-B = -34.74). Our results correspond with the results of Schiettecatte et al. (2007), who found a T/B ratio of 0.74 (T-B = -70). This is, however, in contrast with the results reported by Thomas et al., (2005) who suggested that temperature rather than biological activity controlled the $pCO_{2, sea}$ dynamics seasonally. The data analysed in Thomas et al. (2005) were collected in four short term cruises and one cruise (i.e. in May) did not consider a CO_2 undersaturation (Schiettecatte et al., 2007). This CO_2 undersaturation

215 occurs in the declining phase of the phytoplankton bloom and is typically observed mid–April when the bloom is at its peak in the SBNS (Borges, 2003; Borges and Frankignoulle, 2002; Gypens et al., 2004). Based on our high-temporal-resolution measurements, we found that biological activities in BCS controlled the $pCO_{2, sea}$ and consequently the CO_2 flux (T/B ratio = 0.69). The high-temporal resolution is important to determine the seasonal variations in the $pCO_{2, sea}$, CO_2 flux and their underlying mechanisms. Linking high-temporal-resolution phytoplankton dynamics with our pCO_2 and CO_2 flux data

220 (Hilligsøe et al., 2011) may provide new insights in the CO_2 flux variation and its underlying drivers.

Biogeosciences
Discussions

According to our data in our location, the air–sea CO_2 flux in 2018 was found to be mainly driven by biological processes, and we found that the BCS at our measuring station acted as a sink for atmospheric carbon on an annual scale (-130.19 ± 149.93 mmol C m^{-2} y^{-1}). Our result is in line with other studies, who identified the SBNS as a CO_2 sink on an annual scale (Borges and Frankignoulle, 2002; Gypens et al., 2004; Kitidis et al., 2019; Schiettecatte et al., 2007; Fig. 5).
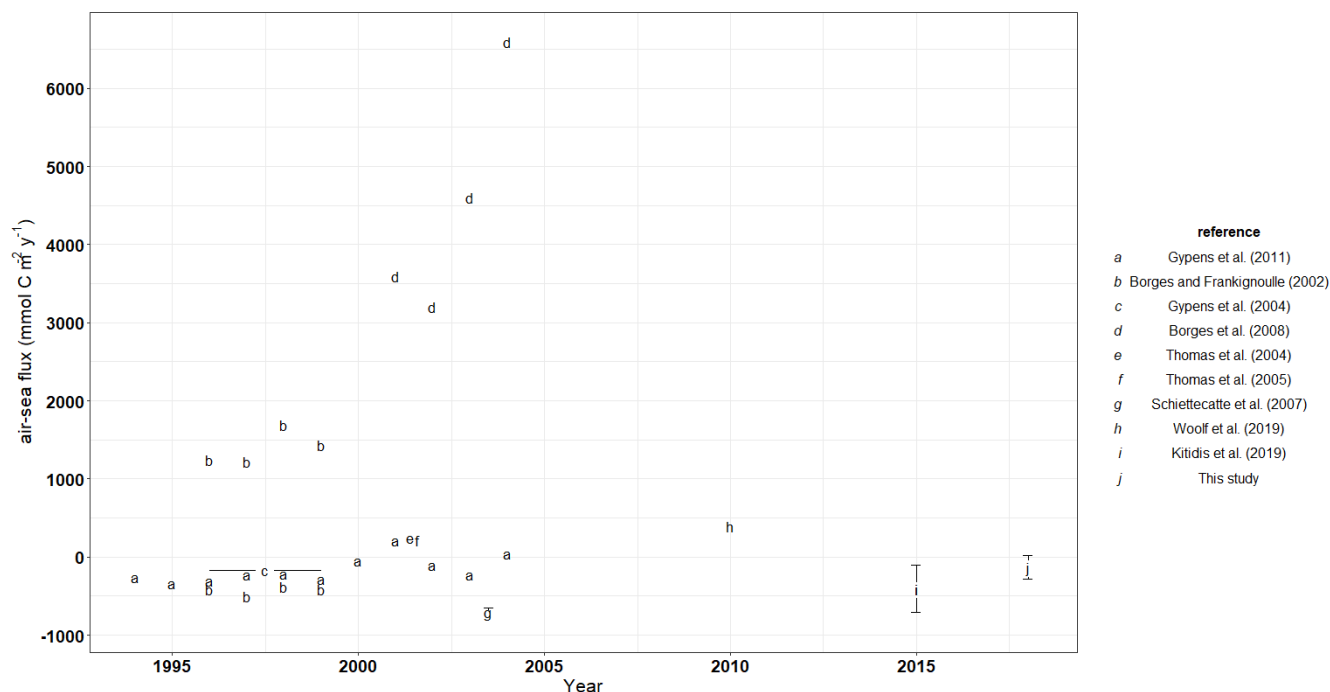

Figure 5: The annual air–sea CO_2 flux from different studies (letter) with data from 1994 to 2018. Studies a, e, f, g, h and i provide an annual air–sea CO_2 flux for the SBNS, whereas studies b, c, d and j for the BCS. Please note that the high values (> 1000 mmol C m^{-2} y^{-1}) of study b and d were located close (< 5 km) to the coast near Zeebrugge. Where possible, the standard deviation (or the standard error in case of study g) is shown by error bars. The horizontal line around a letter indicates that a mean was taken over the indicated period during that study.

Gypens et al. (2004, 2011) simulated annual CO_2 fluxes in range of our findings, e.g. -170 mmol C m^{-2} y^{-1} in 1996 – 1999 and -103 mmol C m^{-2} y^{-1} in 2002. However, the observed annual carbon sinks in other studies were twice (e.g. -300 mmol C m^{-2} y^{-1}; Borges and Frankignoulle, 2002), to four (e.g. -700 mmol C m^{-2} y^{-1}; Schiettecatte et al., 2007), to 20 times as large (e.g. -2000 mmol C m^{-2} y^{-1}; Kitidis et al., 2019) than our quantifications. Indeed, previous studies show a high inter-annual variability in CO_2 flux within the SBNS. Other studies (Borges et al., 2008; Thomas et al., 2004, 2005; Fig. 5) have observed that, in contrast to our study, the southern North Sea was a source of atmospheric CO_2 on an annual scale, e.g. 220 mmol C m^{-2} y^{-1} (Thomas et al., 2005). It should be noted that many of the CO_2 flux data of the southern North Sea are several years old, dating back from 2001–2002 (Thomas et al., 2005), 2003–2004 (Schiettecatte et al., 2007) and 2015 (Kitidis et al., 2019). These previous studies as well as our study show the high inter-annual variability in the BCS. The high inter-annual variability stresses the need to keep track of the air–sea CO_2 flux in a high dynamic area, such as the BCS. Having access to recent and high-temporal-resolution in situ data is important for robust coastal and ocean research but is also useful for policy makers, as

it could refine policy decisions. The carbon fluxes play a major role in the development of the ocean, i.e. ocean acidification (IPCC, 2019) and the global carbon cycle by absorbing anthropogenic carbon emissions (Friedlingstein et al., 2019). Our
245 findings are both in line, i.e. an annual sink for atmospheric carbon, and in contrast, i.e. an annual source for atmospheric carbon, with findings of others studies, demonstrating the high inter-annual variability.

The air–sea CO_2 flux does not only vary in time. It also varies in space. Having data on the spatial variability on a local scale, e.g. Thornton Buoy (this study) and Zeebrugge (Borges et al., 2008; Borges and Frankignoulle, 2002; Fig. 5), could be used
250 to assess the spatial variability within a larger area, such as continental shelf seas. Continental shelf seas showed an increase in absorbing atmospheric CO_2 and variability within the shelf, but also across different shelf systems (Landschützer et al., 2016; Laruelle et al., 2018). Though, it remains uncertain if the increase in atmospheric CO_2 absorption will continue (Legge et al., 2020). As global warming endures, seawater temperature will rise, consequently decreasing the solubility of CO_2 (Wiebe and Gaddy, 1940), reducing the uptake of atmospheric CO_2 (Yamamoto et al., 2018). In addition, global warming can affect
255 the CO_2 uptake indirectly by decreasing or stopping ocean circulation. Less ocean circulation will decrease the nutrient supply, weakening the biological processes and the CO_2 export (Yamamoto et al., 2018). The variability (Laruelle et al., 2018) and insufficient quantification (Legge et al., 2020) of air–sea CO_2 flux stresses the need for more and extensive in situ observations on local, such as in this study, and global scale (Bozec et al., 2006; Wimart–Rousseau et al., 2020; Woolf et al., 2019). High-temporal resolution of CO_2 flux monitoring is key to gain more knowledge about the inter-annual variability, its drivers and
260 the evolution of CO_2 flux. We also suggest extending the observations to investigate the spatial variability in the BCS.

4 Conclusion

We calculated monthly mean air–sea carbon flux at a station in the BCS using high-temporal-resolution data, i.e. daily measured values of $pCO_{2, sea}$ and $pCO_{2, air}$. By doing so, we revealed a large range of the variability in the air–sea carbon flux (-2.99 mmol m^{-2} d^{-1} and 0.37 mmol m^{-2} d^{-1}). The air–sea carbon flux displayed a seasonal pattern, with a sink in the winter–
265 spring months, a source in the summer and a small sink in autumn. We measured a carbon sink for atmospheric CO_2 in 2018 with an estimated uptake of 130.19 ± 149.93 mmol C m^{-2} y^{-1}. We advocate for long-term sustained observations, that will allow to improve the quantification of coastal air–sea CO_2 flux and constrain the associated variations and drivers.

Biogeosciences
Discussions
Open Access
EGU

Appendix A

(a)   (b)
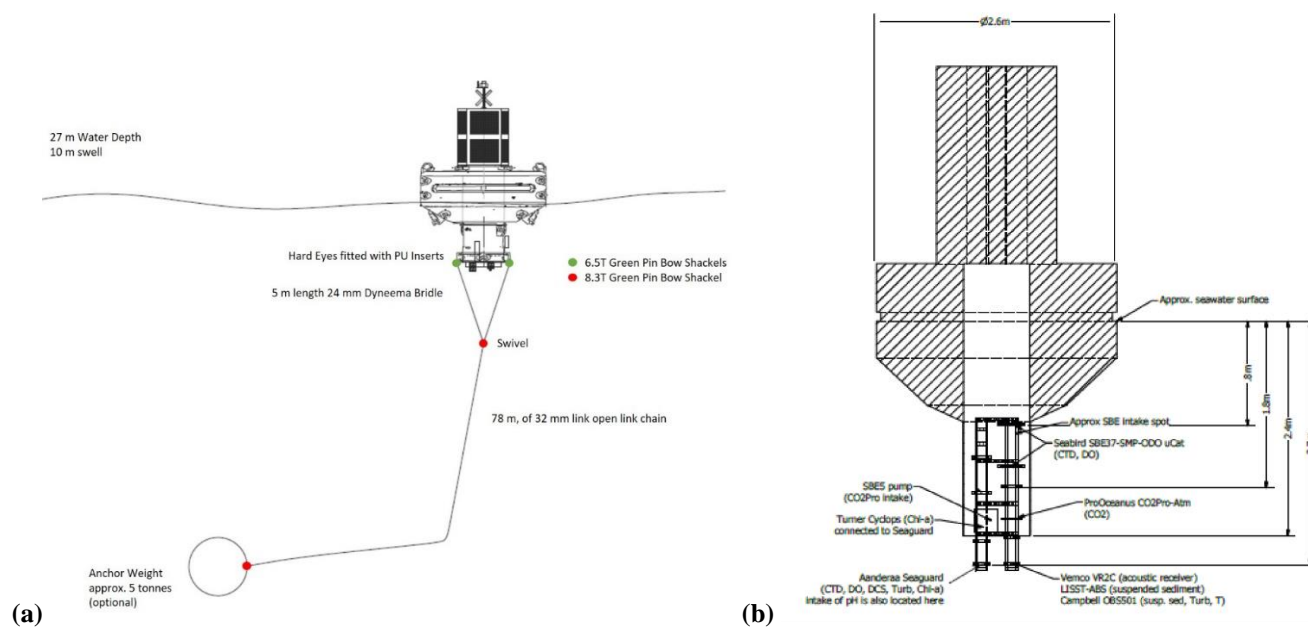
270   **Figure A1: (a) Mooring details and (b) position of the sensors in Thornton Buoy. The sensors used in this study are provided in Table 1.**
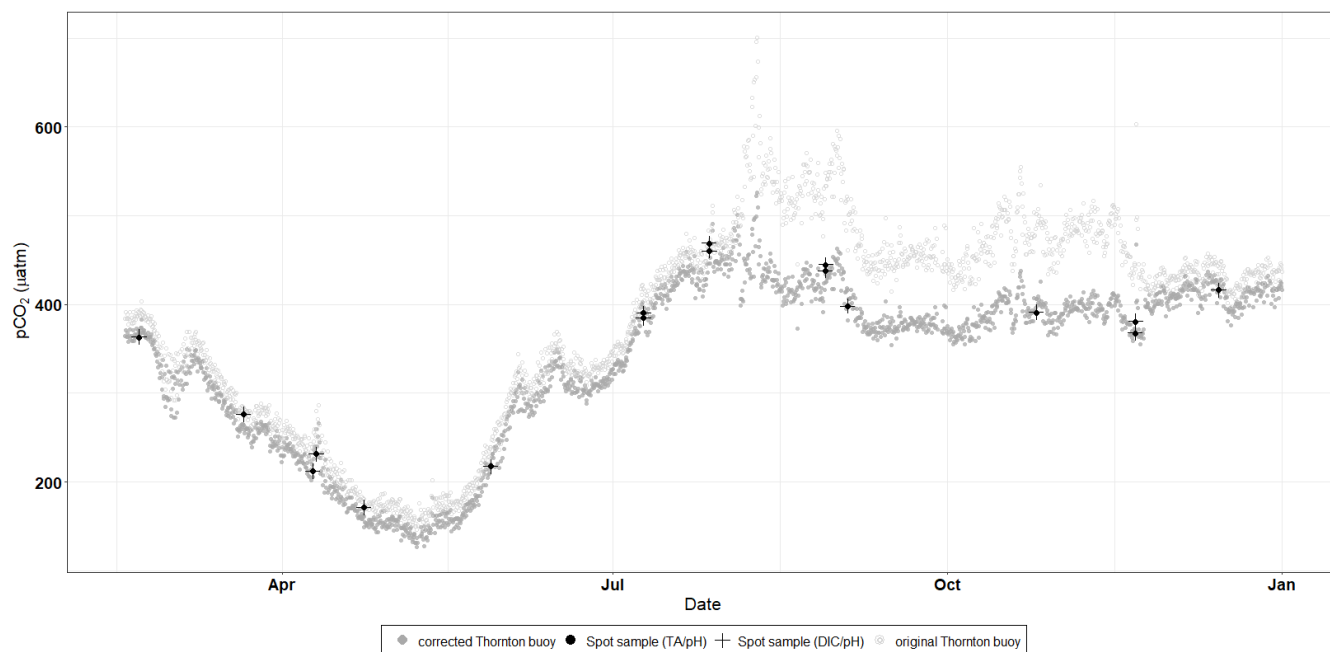

Figure A2: The correction of the Thornton Buoy pCO$_{2,\,sea}$ measurements using a simple linear regression between the buoy's measurements and the spot samples, i.e. TA/pH and DIC/pH.

275 **Data availability**

Data is freely available from the corresponding authors (steven.pint@vliz.be, thanos.gkritzalis@vliz.be) upon request. The data will be available through the ICOS Carbon Portal soon. When available the authors will provide additional information.

Author contributions

Competing interests

The authors declare that they have no conflict of interest.

Acknowledgements

References

290 Arndt, S., Lacroix, G., Gypens, N., Regnier, P. and Lancelot, C.: Nutrient dynamics and phytoplankton development along an estuary-coastal zone continuum: A model study, J. Mar. Syst., 84(3–4), 49–66, doi:10.1016/j.jmarsys.2010.08.005, 2011.

Belpaeme, K., Konings, P. and Vanhooren, S.: Coördinatiepunt Duurzaam Kustbeheer: Oostende, in De kustatlas Vlaanderen/België, edited by K. Belpaeme, P. Konings, and S. Vanhooren, p. 111. [online] Available from: http://www.vliz.be/en/imis?module=ref&refid=207333, 2011.

295 Borges, A. V.: Distribution of surface carbon dioxide and air-sea exchange in the English Channel and adjacent areas, J. Geophys. Res., 108(C5), 1–14, doi:10.1029/2000jc000571, 2003.

Borges, A. V. and Frankignoulle, M.: Distribution and air-water exchange of carbon dioxide in the Scheldt plume off the Belgian coast, Biogeochemistry, 59(1–2), 41–67, doi:10.1023/A:1015517428985, 2002.

Borges, A. V. and Gypens, N.: Carbonate chemistry in the coastal zone responds more strongly to eutrophication than to ocean
300 acidification, Limnol. Oceanogr., 55(1), 346–353, doi:10.4319/lo.2010.55.1.0346, 2010.

Borges, A. V., Schiettecatte, L. S., Abril, G., Delille, B. and Gazeau, F.: Carbon dioxide in European coastal waters, Estuar. Coast. Shelf Sci., 70(3), 375–387, doi:10.1016/j.ecss.2006.05.046, 2006.

Borges, A. V., Ruddick, K., Schiettecatte, L. S. and Delille, B.: Net ecosystem production and carbon dioxide fluxes in the Scheldt estuarine plume, BMC Ecol., 8, 1–10, doi:10.1186/1472-6785-8-15, 2008.

305   Borges, A. V., Royer, C., Lapeyra Martin, J., Champenois, W. and Gypens, N.: Response of marine methane dissolved concentrations and emissions in the Southern North Sea to the European 2018 heatwave, Cont. Shelf Res., 190(November), 104004, doi:https://doi.org/10.1016/j.csr.2019.104004, 2019.

Bozec, Y., Thomas, H., Schiettecatte, L. S., Borges, A. V., Elkalay, K. and De Baar, H. J. W.: Assessment of the processes controlling seasonal variations of dissolved inorganic carbon in the North Sea, Limnol. Oceanogr., 51(6), 2746–2762,

310   doi:10.4319/lo.2006.51.6.2746, 2006.

Delmotte, M., Martin, D., Ramonet, M. and Centre, I. A. T.: Drought-2018 CO2 molar fraction product from Mace Head, , doi:10.18160/DZ94-0WZ7, 2020.

Dickson, A. G., Sabine, C. L. and Christian, J. R.: Guide to best practices for ocean CO2 measurements., PICES Spec. Publ., 3, p191, doi:10.1159/000331784, 2007.

315   Flanders Marine Institute (VLIZ), Belgium: LifeWatch observatory data: nutrient, pigment, suspended matter and secchi measurements in the Belgian Part of the North Sea. https://doi.org/10.14284/393, 2019

Friedlingstein, P., Jones, M. W., O'Sullivan, M., Andrew, R. M., Hauck, J., Peters, G. P., Peters, W., Pongratz, J., Sitch, S., Le Quéré, C., DBakker, O. C. E., Canadell1, J. G., Ciais1, P., Jackson, R. B., Anthoni1, P., Barbero, L., Bastos, A., Bastrikov, V., Becker, M., Bopp, L., Buitenhuis, E., Chandra, N., Chevallier, F., Chini, L. P., Currie, K. I., Feely, R. A., Gehlen, M.,

320   Gilfillan, D., Gkritzalis, T., Goll, D. S., Gruber, N., Gutekunst, S., Harris, I., Haverd, V., Houghton, R. A., Hurtt, G., Ilyina, T., Jain, A. K., Joetzjer, E., Kaplan, J. O., Kato, E., Goldewijk, K. K., Korsbakken, J. I., Landschützer, P., Lauvset, S. K., Lefèvre, N., Lenton, A., Lienert, S., Lombardozzi, D., Marland, G., McGuire, P. C., Melton, J. R., Metzl, N., Munro, D. R., Nabel, J. E. M. S., Nakaoka, S. I., Neill, C., Omar, A. M., Ono, T., Peregon, A., Pierrot, D., Poulter, B., Rehder, G., Resplandy, L., Robertson, E., Rödenbeck, C., Séférian, R., Schwinger, J., Smith, N., Tans, P. P., Tian, H., Tilbrook, B., Tubiello, F. N.,

325   Van Der Werf, G. R., Wiltshire, A. J. and Zaehle, S.: Global carbon budget 2019, Earth Syst. Sci. Data, 11(4), doi:10.5194/essd-11-1783-2019, 2019.

Frumau, A., Hensen, A., Vermeulen, A. and Thematic Centre ICOS Atmosphere: Drought-2018 CO2 molar fraction product from Cabauw, , doi:10.18160/JZAN-9E9K, 2020.

Gattuso, J-P., Epitalon, J-M., Lavigne, H. and Orr, J: seacarb: Seawater Carbonate Chemistry. R package version 3.2.14,

330   https://CRAN.R-project.org/package=seacarb, 2020.

Gypens, N., Lancelot, C. and Borges, A. V.: Carbon dynamics and CO_2 air-sea exchanges in the eutrophied coastal waters of the Southern Bight of the North Sea: a modelling study, Biogeosciences, 1(2), 147–157, doi:10.5194/bg-1-147-2004, 2004.

Gypens, N., Borges, A. V. and Lancelot, C.: Effect of eutrophication on air-sea CO2 fluxes in the coastal Southern North Sea: A model study of the past 50 years, Glob. Chang. Biol., 15(4), 1040–1056, doi:10.1111/j.1365-2486.2008.01773.x, 2009.

14

335   Gypens, N., Lacroix, G., Lancelot, C. and Borges, A. V.: Seasonal and inter-annual variability of air-sea CO2 fluxes and seawater carbonate chemistry in the Southern North Sea, Prog. Oceanogr., 88(1–4), 59–77, doi:10.1016/j.pocean.2010.11.004, 2011.

Hilligsøe, K. M., Richardson, K., Bendtsen, J., Sørensen, L. L., Nielsen, T. G. and Lyngsgaard, M. M.: Linking phytoplankton community size composition with temperature, plankton food web structure and sea-air CO2 flux, Deep. Res. Part I Oceanogr.

340   Res. Pap., 58(8), 826–838, doi:10.1016/j.dsr.2011.06.004, 2011.

Kitidis, V., Shutler, J. D., Ashton, I., Warren, M., Brown, I., Findlay, H., Hartman, S. E., Sanders, R., Humphreys, M., Kivimäe, C., Greenwood, N., Hull, T., Pearce, D., McGrath, T., Stewart, B. M., Walsham, P., McGovern, E., Bozec, Y., Gac, J. P., van Heuven, S. M. A. C., Hoppema, M., Schuster, U., Johannessen, T., Omar, A., Lauvset, S. K., Skjelvan, I., Olsen, A., Steinhoff, T., Körtzinger, A., Becker, M., Lefevre, N., Diverrès, D., Gkritzalis, T., Cattrijsse, A., Petersen, W., Voynova, Y. G., Chapron,

345   B., Grouazel, A., Land, P. E., Sharples, J. and Nightingale, P. D.: Winter weather controls net influx of atmospheric CO2 on the north-west European shelf, Sci. Rep., 9(1), 1–11, doi:10.1038/s41598-019-56363-5, 2019.

Lacroix, G., Ruddick, K., Ozer, J. and Lancelot, C.: Modelling the impact of the Scheldt and Rhine/Meuse plumes on the salinity distribution in Belgian waters (southern North Sea), J. Sea Res., 52(3), 149–163, doi:10.1016/J.SEARES.2004.01.003, 2004.

350   Van Lancker, V., Baeye, M., Evangelinos, D. and Eynde, D.: Monitoring of the impact of the extraction of marine aggregates, in casu sand, in the zone of the Hinder Banks., 2015.

Landschützer, P., Gruber, N. and Bakker, D. C. E.: Decadal variations and trends of the global ocean carbon sink, Global Biogeochem. Cycles, 30, 1396–1417, doi:10.1002/2015GB005359, 2016.

Laruelle, G. G., Cai, W. J., Hu, X., Gruber, N., Mackenzie, F. T. and Regnier, P.: Continental shelves as a variable but

355   increasing global sink for atmospheric carbon dioxide, Nat. Commun., 9(1), 1–11, doi:10.1038/s41467-017-02738-z, 2018.

Legge, O., Johnson, M., Hicks, N., Jickells, T., Diesing, M., Aldridge, J., Andrews, J., Artioli, Y., Bakker, D. C. E., Burrows, M. T., Carr, N., Cripps, G., Felgate, S. L., Fernand, L., Greenwood, N., Hartman, S., Kröger, S., Lessin, G., Mahaffey, C., Mayor, D. J., Parker, R., Queirós, A. M., Shutler, J. D., Silva, T., Stahl, H., Tinker, J., Underwood, G. J. C., Van Der Molen, J., Wakelin, S., Weston, K. and Williamson, P.: Carbon on the Northwest European Shelf: Contemporary Budget and Future

360   Influences, Front. Mar. Sci., 7:143(March), doi:10.3389/fmars.2020.00143, 2020.

Nightingale, D., Malin, G., Law, C. S., Watson, J., Liss, S. and Liddicoat, I.: In situ evaluation of air-sea gas echange parameterizations using novel conservative and volatile tracers, Global Biogeochem. Cycles, 14(1), 373–387, 2000.

O'Doherty, S., Say, D. and Centre, I. A. T.: Drought-2018 CO2 molar fraction product from Tacolneston, doi:10.18160/PDEV-Q5ZM, 2020.

365   IPCC, 2019: IPCC Special Report on the Ocean and Cryosphere in a Changing Climate [H.-O. Pörtner, D.C. Roberts, V. Masson-Delmotte, P. Zhai, M. Tignor, E. Poloczanska, K. Mintenbeck, A. Alegría, M. Nicolai, A. Okem, J. Petzold, B. Rama, N.M. Weyer (eds.)], 2019.

R Core Team: R: A language and environment for statistical computing. R Foundation for Statistical Computing, [online]

Biogeosciences
Discussions

Open Access

EGU

Available from: https://www.r-project.org/, 2019.

370   Salgado, C. M., Azevedo, C., Proença, H. and Vieira, S. M.: Noise Versus Outliers, in Secondary Analysis of Electronic Health
Records, pp. 163–183, Springer International Publishing, Cham., 2016.

Schiettecatte, L. S., Thomas, H., Bozec, Y. and Borges, A. V.: High temporal coverage of carbon dioxide measurements in the
Southern Bight of the North Sea, Mar. Chem., 106(1-2 SPEC. ISS.), 161–173, doi:10.1016/j.marchem.2007.01.001, 2007.

Steinhoff, T., Gkritzalis, T., Lauvset, S. K., Jones, S., Schuster, U., Olsen, A., Becker, M., Bozzano, R., Brunetti, F., Cantoni,

375   C., Cardin, V., Diverrès, D., Fiedler, B., Fransson, A., Giani, M., Hartman, S., Hoppema, M., Jeansson, E., Johannessen, T.,
Kitidis, V., Körtzinger, A., Landa, C., Lefèvre, N., Luchetta, A., Naudts, L., Nightingale, P. D., Omar, A. M., Pensieri, S.,
Pfeil, B., Castaño-Primo, R., Rehder, G., Rutgersson, A., Sanders, R., Schewe, I., Siena, G., Skjelvan, I., Soltwedel, T., van
Heuven, S. and Watson, A.: Constraining the Oceanic Uptake and Fluxes of Greenhouse Gases by Building an Ocean Network
of Certified Stations: The Ocean Component of the Integrated Carbon Observation System, ICOS-Oceans, Front. Mar. Sci.,

380   6(September), 1–15, doi:10.3389/fmars.2019.00544, 2019.

Takahashi, T., Sutherland, S. C., Sweeney, C., Poisson, A., Metzl, N., Tilbrook, B., Bates, N., Wanninkhof, R., Feely, R. A.,
Sabine, C., Olafsson, J. and Nojiri, Y.: Global sea-air CO_2 flux based on climatological surface ocean pCO_2, and seasonal
biological and temperature effects, Deep. Res. Part II Top. Stud. Oceanogr., 49(9–10), 1601–1622, doi:10.1016/S0967-
0645(02)00003-6, 2002.

385   Thomas, H., Bozec, Y., Elkalay, K. and De Baar, H. J. W.: Enhanced Open Ocean Storage of CO_2 from Shelf Sea Pumping,
Science (80-.)., 304, 1005–1008, doi:10.1126/science.1095491, 2004.

Thomas, H., Bozec, Y., Elkalay, K., Baar, H. J. W. De, Borges, A. V and Schiettecatte, L.: Controls of the surface water partial
pressure of the CO_2 in the North Sea, Biogeosciences, 2, 323–334, 2005.

Thomas, H., Prowe, A. E. F., van Heuven, S., Bozec, Y., de Baar, H. J. W., Schiettecatte, L. S., Suykens, K., Koné, M., Borges,

390   A. V., Lima, I. D. and Doney, S. C.: Rapid decline of the CO_2 buffering capacity in the North Sea and implications for the
North Atlantic Ocean, Global Biogeochem. Cycles, 21(4), 1–13, doi:10.1029/2006GB002825, 2007.

Wanninkhof, R.: Relationship between wind speed and gas exchange over the ocean revisited, Limnol. Oceanogr. Methods,
12(JUN), 351–362, doi:10.4319/lom.2014.12.351, 2014.

Watson, A. J., Schuster, U., Bakker, D. C. E., Bates, N. R., Corbière, A., González-Davila, M., Friedrich, T., Hauck, J., Heinze,

395   C., Johannessen, T., Körtzinger, A., Metzl, N., Olafsson, J., Olsen, A., Oschlies, A., Antonio Padin, X., Pfeil, B., Magdalena
Santana-Casiano, J., Steinhoff, T., Telszewski, M., Rios, A. F., Wallace, D. W. R. and Wanninkhof, R.: Tracking the variable
North Atlantic sink for atmospheric CO 2, Science (80-.)., 326(5958), 1391–1393, doi:10.1126/science.1177394, 2009.

Wiebe, R. and Gaddy, V. L.: The Solubility of Carbon Dioxide in Water at Various Temperatures from 12 to 40° and at
Pressures to 500 Atmospheres. Critical Phenomena, J. Am. Chem. Soc., 62(4), 815–817, doi:10.1021/ja01861a033, 1940.

400   Wimart-Rousseau, C., Lajaunie-Salla, K., Marrec, P., Wagener, T., Raimbault, P., Lagadec, V., Lafont, M., Garcia, N., Diaz,
F., Pinazo, C., Yohia, C., Garcia, F., Xueref-Remy, I., Blanc, P. E., Armengaud, A. and Lefèvre, D.: Temporal variability of
the carbonate system and air-sea CO_2 exchanges in a Mediterranean human-impacted coastal site, Estuar. Coast. Shelf Sci.,

236, doi:10.1016/j.ecss.2020.106641, 2020.

Woolf, D. K., Shutler, J. D., Goddijn-Murphy, L., Watson, A. J., Chapron, B., Nightingale, P. D., Donlon, C. J., Piskozub, J.,

405   Yelland, M. J., Ashton, I., Holding, T., Schuster, U., Girard-Ardhuin, F., Grouazel, A., Piolle, J. F., Warren, M., Wrobel-

Niedzwiecka, I., Land, P. E., Torres, R., Prytherch, J., Moat, B., Hanafin, J., Ardhuin, F. and Paul, F.: Key Uncertainties in the

Recent Air-Sea Flux of CO2, Global Biogeochem. Cycles, 0–3, doi:10.1029/2018GB006041, 2019.

Yamamoto, A., Abe-Ouchi, A. and Yamanaka, Y.: Long-term response of oceanic carbon uptake to global warming via

physical and biological pumps, Biogeosciences, 15(13), 4163–4180, doi:10.5194/bg-15-4163-2018, 2018.

410